Density Functional Study of the Migratory Insertion Step in the Carbonylation of Methanol Catalyzed by $[M(CO)_2I_2]^-$ (M = Rh, Ir)

Minserk Cheong,† Rochus Schmid,‡ and Tom Ziegler*

Department of Chemistry, University of Calgary, 2500 University Drive NW, Calgary, Alberta, Canada T2N 1N4

Received December 22, 1999

Quantum-mechanical calculations based on density functional theory (DFT) have been carried out on the migratory insertion process $[M(CO)_2I_3(CH_3)]^- \rightarrow [M(CO)I_3(COCH_3)]^-$ (M = Rh, Ir), which represents an important step in methanol carbonylation. The calculated free energies of activation ($\Delta G^{\ddagger}$) are 27.7 kcal mol^{-1} (Ir) and 17.2 kcal mol^{-1} (Rh), in good agreement with the experimental estimates at 30.6 ± 1.0 kcal mol^{-1} (Ir) and 19.3 ± 0.5 kcal mol^{-1} (Rh). The higher barrier for M = Ir is attributed to a relativistic stabilization of the Ir−CH_3 bond. It is indicated that enthalpic and entropic contributions to $\Delta G^{\ddagger}$ can vary considerably, depending on reaction conditions, without changing $\Delta G^{\ddagger}$ considerably. Especially, simulations based on ab initio molecular dynamics (AIMD) underlined that the reaction system might prefer to trade entropy for enthalpy in polar solutions by dissociating an I^- ligand for M = Ir. A systematic study was also carried out on the general methyl migration reaction $[Ir(CO)_2I_2L(CH_3)]^{n-} \rightarrow [Ir(CO)I_2L(COCH_3)]^{n-}$ ($n = 0, 1$), in which an iodide ligand *trans* to methyl is replaced by another ligand L (where L = CH_3OH, $CH_3C(O)OH$, CO, $P(OCH_3)_3$, SnI_3^-) or an empty coordination site. The free energy of activation for the methyl migration in $[Ir(CO)_2I_2L(CH_3)]$ with L *trans* to methyl follows the order $P(OCH_3)_3$ > CO > SnI_3^-, none > I^- > CH_3OH, $CH_3C(O)OH$ with respect to the ligand L. This order is to a first approximation determined by the ability of L to labilize the M−CH_3 bond *trans* to it. The order is further shaped by the ability of the π-acceptors L = CO, $P(OCH_3)_3$ to stabilize the transition state, and, in the case of L = none, by the relocation of an iodide ligand to the site *trans* to the migrating methyl group. It is finally discussed how placing L *cis* to the migrating CH_3 group might influence the migratory aptitude of methyl.

Introduction

In the late 1960s, workers at Monsanto developed an efficient industrial process for the production of acetic acid. The Monsanto process is based on the carbonylation of methanol by a homogeneous iodide-promoted rhodium catalyst.[1,2] Typical commercial operating conditions are 150−200 °C and 30−100 atm, giving selectivities exceeding 99% based on methanol. A substantial proportion of the 5 million tons of acetic acid made annually uses this process, and the industrial carbonylation of methyl acetate to acetic anhydride also now employs a similar technology.[3−7] The suggested mechanism for the Monsanto process at high iodide concentrations is illustrated[8b,c] in Scheme 1. For the rhodium-based catalyst the oxidative addition of CH_3I to $[Rh(CO)_2I_2]^-$ (**1-[Rh]** of Scheme 1) is rate-determining, whereas the migratory insertion step $[Rh(CO)_2I_3(CH_3)]^-$ (**2-[Rh]**) → $[Rh(CO)I_3(COCH_3)]^-$ (**3-[Rh]**) has a lower barrier.[8b,c] The final reductive elimination of CH_3COI from $[Rh(CO)_2I_3(COCH_3)]^-$ (**4-[Rh]**) appears to be fast, but its rate has not been measured.

Recently BP Chemicals[6,7] has introduced a new catalytic process in which rhodium is replaced by iridium. The new process, named "Cativa", has several advantages over its rhodium-based predecessor, including high reaction rates, good product selectivity, and improved catalyst stability. The carbonylation of methanol catalyzed by rhodium and iridium complexes has been discussed extensively in the literature[9−17] following the pioneering work by Foster.[11,14,15]

Mechanistic studies[8a,18,19] indicate that the iridium system follows the same cycle (Scheme 1) as the

† Permanent address: Department of Chemistry, Kyung Hee University, Seoul 130-701, Korea.

‡ Present address: Technische Universität München, Anorganisch-Chemisches Institut, D-85747 Garching, Germany.

(1) Paulik, F. E.; Roth, J. F. *J. Chem. Soc., Chem. Commun.* **1968**, 1578.
(2) Roth, J. F.; Craddock, J. H.; Hershman, A.; Paulik, F. E. *Chem. Technol.* **1971**, 600.
(3) Polichnowski, S. W. *J. Chem. Educ.* **1986**, *63*, 204.
(4) Agreda, V. H. *Chem. Technol.* **1988**, 250.
(5) Zoeller, J. R.; Agreda, V. H.; Cook, S. L.; Lafferty, N. L.; Polichnowski, S. W.; Pond, D. M. *Catal. Today* **1992**, *13*, 73.
(6) *Chem. Br.* **1996**, *32*, 7.
(7) *Chem. Ind. (London)* **1996**, 483.
(8) (a) Ghaffar, T.; Adams, H.; Maitlis, P. M.; Sunley, G. J.; Baker, M. J.; Haynes, A. *Chem. Commun.* **1998**, 1023. (b) Haynes, A.; Mann, B. E.; Gulliver, D. J.; Morris, G. E.; Maitlis, P. M. *J. Am. Chem. Soc.* **1991**, *113*, 8567. (c) Haynes, A.; Mann, B. E.; Morris, G. E.; Maitlis, P. M. *J. Am. Chem. Soc.* **1993**, *115*, 4093. (d) Griffin, T. R.; Cook, D. B.; Haynes, A.; Pearson, J. M.; Monti, D.; Morris, G. E. *J. Am. Chem. Soc.* **1996**, *118*, 3029.
(9) Brodzki, D.; Denise, B.; Pannetier, G. *J. Mol. Catal.* **1977**, *2*, 149.
(10) Matsumoto, T.; Mizoroki, T.; Ozaki, A. *J. Catal.* **1978**, *51*, 96.
(11) Forster, D. *Adv. Organomet. Chem.* **1979**, *17*, 255.

10.1021/om9910221 CCC: $19.00
Publication on Web 04/18/2000

Scheme 1. Proposed Catalytic Cycle for Carbonylation of CH_3OH Catalyzed by $[M(CO)_2I_2]^-$ (Adapted from Ref 8b)

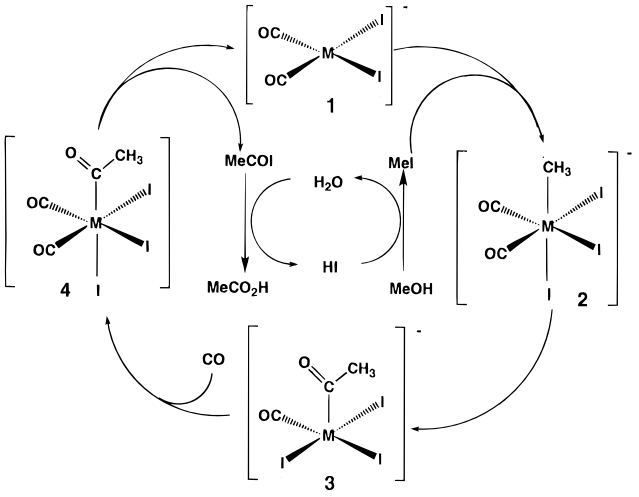

rhodium homologue at high iodide concentrations. However, oxidative addition of methyl iodide (**1** → **2**) is 100 times faster for iridium than for rhodium, whereas the migratory insertion step (**2** → **3**) is up to 10^6 times slower for the heavier metal.[13,16,17] As a result, the migratory insertion step (**2** → **3**) becomes rate-determining in the Cativa process. The difference in relative rates between the two metals is a reflection of the stronger iridium−carbon bond.

Several experimental studies have explored ways in which to reduce the barrier for the rate-determining migratory insertion step (**2** → **3**) of the iridium system by ligand substitution and solvent modifications.[18,19] We approach here the same objective by conducting a systematic theoretical study on the migratory insertion step (**2** → **3**). Our theoretical investigation explores in the first place the differences between rhodium and iridium in the migratory insertion step involving $[M(CO)_2I_3(CH_3)]^-$ (**2**). We assess next how the insertion barrier is changed for iridium by substituting the iodide ligand *trans* to the methyl group with other ligands L (where L = CH_3OH, $CH_3C(O)OH$, CO, $P(OCH_3)_3$, SnI_3^-) or an empty coordination site. Considerations will also be given to the role of the solvent. Where possible, our calculated results will be compared to experimental data. Previous theoretical studies have dealt with migratory insertion processes[20−26] involving CO and methyl. However, this is to our knowledge the first systematic study of the migratory insertion process of direct relevance for the iridium-based carbonylation of methanol. A brief theoretical note on the corresponding addition reaction (**1** → **2**) has appeared.[8d]

Computational Details

Stationary points on the potential energy surface were calculated using the Amsterdam density functional (ADF) program, developed by Baerends et al.[27,28] and vectorized by Ravenek.[29] The numerical integration scheme applied for the calculations was developed by te Velde et al.[30,31] The geometry optimization procedure was based on the method of Versluis and Ziegler.[32] The electronic configurations of the molecular systems were described by double-ζ STO basis sets with polarization functions for the H, C, and O atoms, while triple-ζ Slater type basis sets were employed for the P, Rh, Sn, I, and Ir atoms.[33,34] The 1s electrons of C and N, the 1s−2p electrons of P, the 1s−3d electrons of Rh, the 1s−4p electrons of Sn and I, and the 1s−4f electrons of Ir were treated as frozen cores. A set of auxiliary[35] s, p, d, f, and g STO functions, centered on all nuclei, was used in order to fit the molecular density and the Coulomb and exchange potentials in each SCF cycle. Energy differences were calculated by augmenting the local exchange-correlation potential by Vosko et al.[36] with Becke's[37] nonlocal exchange corrections and Perdew's[38] nonlocal correlation corrections (BP86). Geometries were optimized including nonlocal corrections, and the harmonic vibrational frequencies were also computed at this level of theory. Thermodynamic properties were evaluated according to standard textbook procedures.[39] Solvation free energies were calculated using the conductor-like screening model (COSMO) of Klamt and Schüürmann,[40] which has been recently implemented into the ADF package.[41] To compare with experimental results, chlorobenzene ($\epsilon_0 = 5.62$) was used for iridium complexes and iodomethane ($\epsilon_0 = 7.00$) was used for rhodium complexes as a solvent. First-order Pauli scalar relativistic corrections[42,43] were added variationally to the total energy for all systems. In view of the fact that all systems investigated in this work

(12) Dekleva, T. W.; Forster, D. *Adv. Catal.* **1986**, *34*, 81.
(13) Maitlis, P. M.; Haynes, A.; Sunley, G. J.; Howard, M. J. *J. Chem. Soc., Dalton Trans.* **1996**, 2187.
(14) Forster, D. *J. Chem. Soc., Dalton Trans.* **1979**, 1639.
(15) Forster, D.; Singleton, T. C. *J. Mol. Catal.* **1982**, *17*, 299.
(16) Ellis, P. R.; Pearson, J. M.; Haynes, A.; Adams, H.; Bailey, N. A.; Maitlis, P. M. *Organometallics* **1994**, *13*, 3215.
(17) Bassetti, M.; Monti, D.; Haynes, A.; Pearson, J. M.; Stanbridge, I. A.; Maitlis, P. M. *Gazz. Chim. Ital.* **1992**, *122*, 391.
(18) Haynes, A.; Pearson, J. M.; Vickers, P. W.; Charmant, J. P. H.; Maitlis, P. M. *Inorg. Chim. Acta* **1998**, *270*, 382.
(19) Pearson, J. M.; Haynes, A.; Morris, G. E.; Sunley, G. J.; Maitlis, P. M. *J. Chem. Soc., Chem. Commun.* **1995**, 1045.
(20) Sakaki, S.; Kitaura, K.; Morokuma, K.; Ohkubo, K. *J. Am. Chem. Soc.* **1983**, *105*, 2280.
(21) (a) Koga, N.; Morokuma, K. *J. Am. Chem. Soc.* **1985**, *107*, 7230. (b) Koga, N.; Morokuma, K. *J. Am. Chem. Soc.* **1986**, *108*, 6136. (c) Koga, N.; Morokuma, K. *New J. Chem.* **1991**, *15*, 749. (d) Matsubara, T.; Koga, N.; Ding, Y.; Musaev, D. G.; Morokuma, K. *Organometallics* **1997**, *16*, 1065.
(22) Rappé, A. K. *J. Am. Chem. Soc.* **1987**, *109*, 5605.
(23) Blomberg, M. R. A.; Karlsson, C. A. M.; Siegbahn, P. E. M. *J. Phys. Chem.* **1993**, *97*, 9341.
(24) (a) Axe, F. U.; Marynick, D. S. *Organometallics* **1987**, *6*, 572. (b) Axe, F. U.; Marynick, D. S. *J. Am. Chem. Soc.* **1988**, *110*, 3728.
(25) Ziegler, T.; Versluis, L.; Tschinke, V. *J. Am. Chem. Soc.* **1986**, *108*, 612.
(26) Versluis, L.; Ziegler, T. *J. Am. Chem. Soc.* **1989**, *111*, 2018.
(27) Baerends, E. J.; Ellis, D. E.; Ros, P. *Chem. Phys.* **1973**, *2*, 41.
(28) Baerends, E. J.; Ros, P. *Chem. Phys.* **1973**, *2*, 52.
(29) Ravenek, W. *Algorithms and Applications on Vector and Parallel Computers*; te Riele, H. J. J., Dekker, T. J., van de Horst, H. A., Eds.; Elsevier: Amsterdam, The Netherlands, 1987.
(30) te Velde, G.; Baerends, E. J. *J. Comput. Chem.* **1992**, *99*, 84.
(31) Boerrigter, P. M.; Velde, G. t.; Baerends, E. J. *Int. J. Quantum Chem.* **1988**, *33*, 87.
(32) Versluis, L.; Ziegler, T. *J. Chem. Phys.* **1988**, *88*, 322.
(33) Snijders, J. G.; Baerends, E. J.; Vernoijs, P. *At. Nucl. Data Tables* **1982**, *26*, 483.
(34) Vernoijis, P.; Snijders, J. G.; Baerends, E. J. Slater Type Basis Functions for the Whole Periodic System; Internal Report (in Dutch); Department of Theoretical Chemistry, Free University: Amsterdam, The Netherlands, 1981.
(35) Krijn, J.; Baerends, E. J. Fit Functions in the HFS Method; Internal Report (in Dutch); Department of Theoretical Chemistry, Free University: Amsterdam, The Netherlands, 1984.
(36) Vosko, S. H.; Wilk, L.; Nusair, M. *Can. J. Phys.* **1980**, *58*, 1200.
(37) Becke, A. *Phys. Rev. A* **1988**, *38*, 3098.
(38) (a) Perdew, J. P. *Phys. Rev. B* **1986**, *34*, 7406. (b) Perdew, J. P. *Phys. Rev. B* **1986**, *33*, 8822.
(39) McQuarrie, D. A. *Statistical Thermodynamics*; Harper & Row: New York, 1973.
(40) Klamt, A.; Schüürmann, G. *J. Chem. Soc., Perkin Trans. 2* **1993**, 799.
(41) (a) Pye, C. C.; Ziegler, T. *Theor. Chem. Acta* **1999**, *101*, 396. (b) Margel, P.; et al. To be submitted for publication.
(42) Snijders, J. G.; Baerends, E. J. *Mol. Phys.* **1978**, *36*, 1789.
(43) Snijders, J. G.; Baerends, E. J.; Ros, P. *Mol. Phys.* **1979**, *38*, 1909.

show a large HOMO−LUMO gap, a spin-restricted formalism was used for all calculations. No symmetry constraints were used. The transition states were fully optimized with one imaginary frequency.

All reported molecular dynamics simulations were carried out with the Car−Parrinello projector-augmented-wave (CP-PAW) code developed by Blöchl.[44] The wave function is expanded in plane waves up to an energy cutoff of 30 Ry. The frozen-core approximation was applied for the same shells as in the ADF calculations. We use periodic boundary conditions with a 12 Å fcc cell. All simulations were performed using the local density approximation in the parametrization of Perdew and Zunger,[45] with the gradient corrections of Becke[37] and Perdew.[38] Long-range electrostatic interactions between different cells are eliminated using a method developed by Blöchl,[44] which is based on fitting an atom-centered Gaussian charge density to the molecular electronic density.[46] A time step of 10 au is used, correcting the mass of the nuclei to account for the drag of the electrons in the coupled dynamics integrated with the Verlet algorithm. The temperature of the nuclei is controlled by a Nosé[48] thermostat, which creates a canonical (NVT) ensemble. All simulations were conducted at 300 K. To sample phase space in the vicinity of the transition state, we have chosen a reaction coordinate (RC) which is kept constrained during the dynamics using SHAKE[49] constraints. It is desirable that the RC has a high projection onto the IRC[50] (intrinsic reaction coordinate). All other degrees of freedom are allowed to evolve naturally in time. When the constraint is slowly varied, phase space in the vicinity of the transition state can be sampled dynamically,[51] leading to undisturbed dynamics for all motions which are orthogonal to the RC and to fictitious dynamics along the RC. This makes it possible to investigate even high-lying transition states, such as those encountered in the present study. To achieve an evenly distributed thermal excitation, the dynamics were initialized with vibrational eigenvectors taken from ADF calculations; the nuclei were slowly heated with a sinusoidal pulse to avoid detachment of the electrons from the Born−Oppenheimer surface by abrupt changes in the nuclear velocities.

Integrating the force along the reaction coordinate (RC) is a possible way to determine the free energy ΔF of the reaction as

$$\Delta F = \int_0^1 \left(\frac{\partial E}{\partial \lambda}\right)_{\lambda,T} \mathrm{d}\lambda \qquad (1)$$

where λ is just the reaction coordinate running between 0, at the beginning of the reaction, and 1, at the end of the reaction. Further, the integrand is the appropriately scaled averaged force on the reaction coordinate sampled at constant temperature and λ. A very convenient way to determine the above integral is to change the reaction coordinate λ continuously from 0 to 1 and to only record a single value of $\partial E/\partial\lambda$ at one given λ. This technique is called the "slow growth" method. Relativistic effects were included in the same way as for the static ADF calculations.[42,43] Solvation effects were included dynamically[41b] within the COSMO[40] formalism.

Results and Discussion

Our discussion of the migratory insertion process is divided into two parts. The first deals with the generic

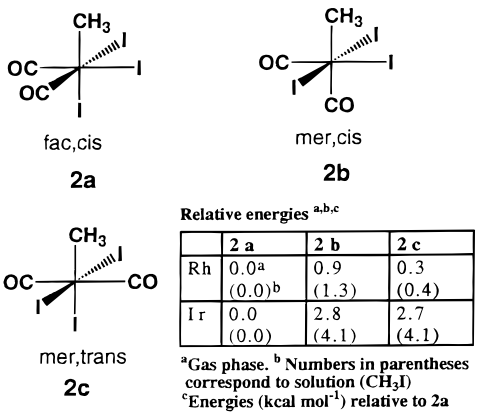

Relative energies [a,b,c]

	2 a	2 b	2 c
Rh	0.0[a] (0.0)[b]	0.9 (1.3)	0.3 (0.4)
Ir	0.0 (0.0)	2.8 (4.1)	2.7 (4.1)

[a]Gas phase. [b] Numbers in parentheses correspond to solution (CH_3I)
[c]Energies (kcal mol^{-1}) relative to 2a

Figure 1. Isomers of $[M(CO)_2I_3(CH_3)]^-$ and their relative energies.

$[M(CO)_2I_3(CH_3)]^-$ system for M = Rh, Ir. The second part discusses how the rate of migratory insertion is changed by substituting the I^- ligand *trans* to methyl by another ligand L (where L = CH_3OH, $CH_3C(O)OH$, CO, $P(OCH_3)_3$, SnI_3^-) or an empty coordination site.

1. Migratory Insertion Involving $[M(CO)_2I_3(CH_3)]^-$ (M = Rh, Ir). We shall first discuss the basic migratory insertion process

$$[M(CO)_2I_3(CH_3)]^- \rightarrow [M(CO)I_3(COCH_3)]^- \qquad M = \mathrm{Rh, Ir} \quad (2)$$

with an emphasis on the difference between the two metals. The process in eq 2 will be analyzed on the basis of static as well as dynamic DFT calculations.

A. Static Calculations. The $[M(CO)_2I_2]^-$ catalyst (**1**; M = Rh, Ir) has a square-planar geometry with a d^8 low-spin configuration. The structure with CO and iodide in *cis* positions was preferred over the corresponding *trans* isomer by 8.2 kcal mol^{-1} (Rh) and 15. 1 kcal mol^{-1} (Ir) in the gas phase, as one would expect from the stronger *trans*-directing effect of the CO ligand and the facile donation of π-electrons from iodide to CO. The energy difference is enhanced slightly in solution (CH_3I) to 8.8 kcal mol^{-1} (Rh) and 16.0 kcal mol^{-1} (Ir), due to the net dipole moment of the *cis* isomer. The oxidative addition product $[M(CO)_2I_3(CH_3)]^-$ (**2**; M = Rh, Ir) from the reaction between CH_3I and $[M(CO)_2I_2]^-$ (**1**) has three possible isomers (see Figure 1) and a d^6 low-spin configuration. We find the *fac*,*cis* isomer **2a** to be the most stable conformation for both metals in solution as well as in the gas phase. However, for rhodium the *mer*,*trans* isomer **2c** is only marginally less stable, as shown in Figure 1.

In the migratory process of eq 2 the methyl group moves from the metal center to the *cis* carbonyl carbon. In the process the methyl carbon slides parallel to the M−CO bond vector (**c** of Figure 2) while the local methyl C_3 axis rotates from a direction toward the metal to a direction toward the *cis* carbonyl carbon. At the same time the *cis* carbonyl CO distance (**d**) is stretched and the M−C−O angle (**cd**) reduced from 180° to between 105 and 110°. Finally, the M−L bond (**e**) is shortened as the CH_3 leaves the site *trans* to L, whereas the M−I bond (**f**) *trans* to the emerging and strongly *trans*-directing acyl group is elongated. The optimized bond distances and bond angles for **2** and **TS[2-3]** are given in Tables 1 and 2, respectively.

(44) Blöchl, P. E. *J. Chem. Phys.* **1995**, *103*, 7422.
(45) Perdew, J. P.; Zunger, A. *Phys. Rev. B* **1981**, *23*, 5048.
(46) Blöchl, P. E.; Parrinello, M. *Phys. Rev. B* **1992**, *45*, 9413.
(47) Verlet, L. *Phys. Rev.* **1967**, *159*, 98.
(48) (a) Nosé, S. *Mol. Phys.* **1984**, *52*, 255. (b) Hoover, W. G. *Phys. Rev. A* **1985**, *31*, 1695.
(49) Ryckaert, J.-P.; Ciccotti, G.; Berendsen, H. J. *J. Comput. Phys.* **1977**, *23*, 327.
(50) Fukui, K. *Acc. Chem. Res.* **1981**, *14*, 363.
(51) Straatsma, T. P.; Berendsen, H. J. C.; Postma, J. P. M. *J. Chem. Phys.* **1986**, *85*, 6720.

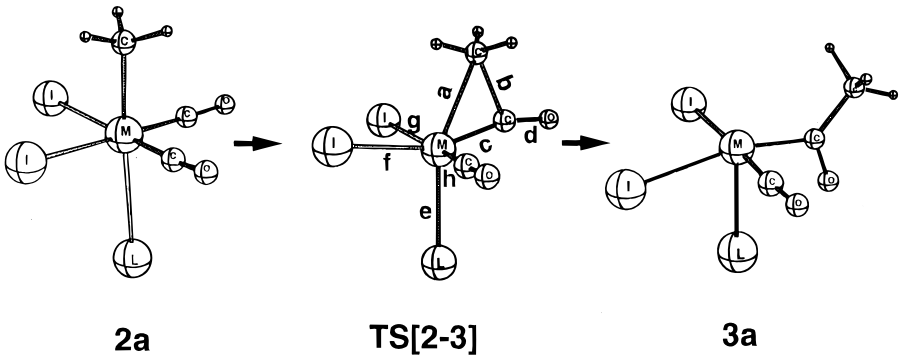

Figure 2. Key structures in the migratory insertion process.

Table 1. Optimized Bond Distances[a] in the Reactants (2) and Transition States (TS[2-3]) for Migratory Insertion in $[M(CO)_2I_2(CH_3)L]^{n-}$

			reactant					transition state				
M	L[b]		M−CH_3 **a**[b]	M−CO **h/c**	M−I **g/f**	M−L **e**	H_3C−CO **b**	M−CH_3 **a**	M−CO[c] **h (c)**	M−I[d] **g (f)**	M−L **e**	H_3C−CO **b**
Ir	**I**	I^-	2.17	1.87	2.82	2.94	2.87	2.50	1.86 (1.89)	2.81 (2.90)	2.77	1.88
	II	*f*	2.14	1.88	2.73		2.79	2.43	1.89 (1.87)	2.72 (2.68[e])		1.84
	III	CH_3OH	2.13	1.88	2.78	2.39	2.80	2.35	1.89 (1.91)	2.76 (2.91)	2.17	1.70
	IV	$CH_3C(O)OH$	2.13	1.88	2.78	2.48	2.80	2.36	1.89 (1.91)	2.78 (2.89)	2.17	1.70
	V	*C*O	2.18	1.90	2.82	2.00	2.77	2.43	1.92 (1.92)	2.79 (2.86)	1.88	1.88
	VI	$P(OCH_3)_3$	2.19	1.89	2.83	2.38	2.80	2.44	1.89 (1.90)	2.79 (2.88)	2.22	1.92
	VII	SnI_3^-	2.18	1.88	2.80	2.79	2.83	2.50	1.87 (1.90)	2.80 (2.87)	2.63	1.92
Rh	**VIII**	I^-	2.15	1.87	2.81	2.94	2.85	2.39	1.87 (1.87)	2.80 (2.91)	2.77	1.91
	IX	f	2.11	1.89	2.72		2.78	2.34	1.90 (1.85)	2.71 (2.67[d])		1.92
	X	*C*O	2.16	1.91	2.81	2.01	2.74	2.36	1.92 (1.89)	2.78 (2.87)	1.90	1.92

[a] Distances are in Å. [b] Ligand in *trans* position to methyl group. Ligating atoms are shown in boldface italic type, and the Roman numbering codes used for the complexes are also shown. The boldface letter associated with each distance refers to the index in Figure 2. [c] Numbers in parentheses are bond distances to the CO ligand to which the methyl group is migrating. [d] Numbers in parentheses are bond distances to the I^- ligand *trans* to emerging acyl group. [e] Since the structure of this compound is not octahedral in the reactant, the I^- ligand is not in the *trans* position to the emerging acyl group. [f] No ligand L in *trans* position to methyl group.

Table 2. Optimized Bond Angles[a] in the Reactants (2) and Transition States (TS[2−3]) for Migratory Insertion in $[M(CO)_2I_2(CH_3)L]^{n-}$

		reactant				transition state			
M	L[b]	L−M-CH_3 **ea**[b]	H_3C−M−CO **ah/ac**	H_3C−M-I **ag/af**	M−C−O **cd**	L−M−CH_3 **ea**	H_3C−M−CO[c] **ah (ac)**	H_3C−M−I[d] **ag (af)**	M−C−O[c] **cd**
Ir	I^-	176.7	90.4	88.8	176.1	153.4	95.0 (48.2)	85.3 (108.6)	161.0
	e		87.9	100.6	176.6		92.0 (48.7)	90.0 (170.3)	159.5
	CH_3OH	177.4	88.4	93.5	177.0	155.6	93.3 (45.4)	87.8 (126.4)	154.3
	$CH_3C(O)OH$	178.2	88.3	92.6	176.9	152.2	94.1 (45.4)	88.3 (117.5)	154.6
	*C*O	174.2	85.1	89.8	176.6	158.9	91.4 (49.5)	90.4 (100.6)	162.0
	$P(OCH_3)_3$	178.0	86.3	87.4	177.0	157.2	91.8 (50.8)	86.9 (99.6)	162.7
	SnI_3^-	177.8	88.1	90.2	176.0	152.0	94.3 (49.6)	88.6 (105.6)	162.4
Rh	I^-	173.9	89.4	89.2	175.5	159.4	96.2 (51.7)	87.6 (99.2)	163.2
	e		87.8	100.5	175.8		92.5 (52.8)	89.9 (165.9)	163.1
	*C*O	173.8	84.5	90.3	176.0	162.6	92.2 (52.5)	89.6 (101.0)	164.0

[a] Angles are in degrees. [b] Ligand in *trans* position to methyl group. The boldface letter associated with each angle refers to the index in Figure 2. [c] Numbers in parentheses are bond angles to the CO ligand to which the methyl group is migrating. [d] Numbers in parentheses are bond angles to the I^- ligand *trans* to the emerging acyl group. [e] No ligand L in *trans* position.

The calculated free energies of activation ($\Delta G^{\ddagger}$) for the process in eq 2 are 29.2 kcal mol^{-1} (Ir) and 18.4 kcal mol^{-1} (Rh) in the gas phase compared to 27.7 kcal mol^{-1} (Ir) and 17.2 kcal mol^{-1} (Rh) in solution, as shown in Table 3. The solution values are in good agreement with the experimental estimates at 30.6 ± 1.0 kcal mol^{-1} (Ir)[19] and 19.3 ± 0.5 kcal mol^{-1} (Rh).[8c] Thus, our calculations reproduce well the reduction in $\Delta G^{\ddagger}$ from iridium to rhodium. The reduction reflects the fact that relativistic effects make the M−CH_3 bond stronger for the heavier metal (iridium). Solvent effects are seen to reduce $\Delta G^{\ddagger}$ slightly as the transition state **TS[2-3]** is more polar than the reactant **2**.

The agreement between experiment and theory for the individual components $\Delta H^{\ddagger}$ and $\Delta S^{\ddagger}$ to $\Delta G^{\ddagger} = \Delta H^{\ddagger} - T\Delta S^{\ddagger}$ is not as good as for $\Delta G^{\ddagger}$ itself. For rhodium we find $\Delta H^{\ddagger} = 17.5$ kcal mol^{-1} and $\Delta S^{\ddagger} = 1.06$ cal mol^{-1} K^{-1} compared to the experimental estimates[8c] of $\Delta H^{\ddagger} = 15.0 \pm 0.5$ kcal mol^{-1} and $\Delta S^{\ddagger} = -14.1 \pm 2.2$ cal mol^{-1} K^{-1}, respectively. We interpret the difference in terms of explicit solvent involvement during the migratory insertion, an effect not easily considered in our model. The explicit solvent involvement might lower $\Delta H^{\ddagger}$ at the expense of increasing $-T\Delta S^{\ddagger}$. The result could be a modest decrease in $\Delta G^{\ddagger}$ and much larger (compensating) changes in the components $\Delta H^{\ddagger}$ and $\Delta S^{\ddagger}$. Large variations in $\Delta H^{\ddagger}$ and $\Delta S^{\ddagger}$ without any notable change in $\Delta G^{\ddagger}$ have been observed to take place for a given reaction when external factors (such as solvents) are changed.

Table 3. Activation Parameters[a] for the CO Insertion in $[M(CO)_2I_2(CH_3)L]^{n-}$

M	L[b]	$\Delta S^{\ddagger}$(g)[c]	$\Delta H^{\ddagger}$(g)[c]	$\Delta G^{\ddagger}$(g)[c]	$\Delta H^{\ddagger}$(s)[d]	$\Delta G^{\ddagger}$(s)[e]	$\Delta S^{\ddagger}$(exptl)[f]	$\Delta H^{\ddagger}$(exptl)[f]	$\Delta G^{\ddagger}$(exptl)[f]
Ir		−5.19	22.7	24.2	21.2[g]	22.7[g]			
	I$^-$	2.02	29.8	29.2	28.3	27.7	21.8 ± 1.9[h]	37.0 ± 1.0[h]	30.6 ± 1.0[h]
	CH_3***O***H	−5.70	36.5	38.2	33.1	34.8			
	CH_3C(***O***)OH	−4.74	39.5	40.9	34.2	35.6			
	CO	−3.90	18.7	19.8	17.3	18.5	−8.6 ± 1.9[i]	21.3 ± 0.7[i]	23.8 ± 0.7[i]
	P$(OCH_3)_3$	1.92	17.2	16.6	13.9	13.3			
	SnI_3^-	−3.80	23.3	24.4	22.1	23.3			
Rh		−3.63	15.8	16.9	14.6	15.7			
	I$^-$	1.06	18.7	18.4	17.5	17.2	−14.1 ± 2.2[j]	15.0 ± 0.5[j]	19.3 ± 0.5[j]
	CO	−3.75	12.6	13.7	11.6	12.7			

[a] At 298.15 K and 1 atm. All energies are in kcal mol^{-1} and entropies in cal K^{-1} mol^{-1}. The barrier calculated is that from a reactant isomer (**2a**) to **TS[2-3]**. [b] Ligand in *trans* position to methyl group. [c] $\Delta S^{\ddagger}$(g), $\Delta H^{\ddagger}$(g), and $\Delta G^{\ddagger}$(g) are $\Delta S^{\ddagger}$, $\Delta H^{\ddagger}$, and $\Delta G^{\ddagger}$ from gas-phase calculations. [d] $\Delta H^{\ddagger}(s) = \Delta H^{\ddagger}(g) + \Delta H^{el}(s)$. Here $\Delta H^{el}(s)$ is the electrostatic solvation stabilization.[41a] [e] $\Delta G^{\ddagger}(s) = \Delta H^{\ddagger}(s) - T\Delta S^{\ddagger}(g)$ [f] Experimental numbers are obtained in solution. Solvents are chlorobenzene for iridium and iodomethane for rhodium. The same solvents are used in theoretical calculations. [g] 25% CH_3OH in PhCl. [h] Reference 19. [i] Reference 8a. [j] Reference 8c.

This change has been referred to as an isokinetic response.[52,53]

The difference between the observed and calculated components $\Delta H^{\ddagger}$ and $\Delta S^{\ddagger}$ is even larger for iridium. Here $\Delta S^{\ddagger}$ is observed[19] to have a large positive value of 21.8 ± 1.9 cal mol^{-1} K^{-1} compared to our estimate of 2.02 cal mol^{-1} K^{-1}. On the other hand, experiment[19] finds a large activation enthalpy of $\Delta H^{\ddagger} = 37.0 \pm 1.0$ kcal mol^{-1} compared to our lower estimate of 28.3 kcal mol^{-1}. We shall demonstrate in the next section that a possible isokinetic response responsible for the difference in calculated and observed $\Delta H^{\ddagger}$ and $\Delta S^{\ddagger}$ values is the entropically driven dissociation of a I^- ligand during the insertion process. Such a process is not taken into account in our static calculations as they are presented here.

The coordinatively unsaturated low-spin d^6 acyl complex $[M(CO)I_3(COCH_3)]^-$ (**3**; M = Rh, Ir) resulting from the migratory insertion process can adopt three basic square-pyramidal conformations with respectively I^- (**3a**), CO (**3b**), or $COCH_3$ (**3c**) in the apical position. We find for both metals that **3c** is the most stable isomer. Depending on the metal and the acyl orientation **3b** is found to be 8.8−11.6 kcal mol^{-1} higher in energy, whereas **3a** is 12.8−19.3 kcal mol^{-1} above **3c**.

We find that the insertion reaction (**2a** → **3c**) is endergonic for iridium and exergonic for rhodium, as shown in Table 4. This trend reflects the relativistic stabilization of the Ir−CH_3 bond relative to the Rh−CH_3 linkage. Experimental data[8c] are available for rhodium with $\Delta G = -5.0$ kcal mol^{-1} compared to our calculated value of −6.2 kcal mol^{-1}. The individual experimental components of $\Delta S = -12$ cal K^{-1} mol^{-1} and $\Delta H = -8.8$ kcal mol^{-1} differ again from our calculated estimates (without explicit solvation effects) of $\Delta S = 2.2$ cal K^{-1} mol^{-1} and $\Delta H = -5.6$ kcal mol^{-1} in a way that suggests explicit solvent stabilization of the coordinatively unsaturated complex **3c**.

B. Dynamic Calculations. We have carried out an ab initio molecular dynamics (AIMD) simulation of the migratory insertion reaction involving $[Ir(CO)_2I_3(CH_3)]^-$ with the aid of the Car−Parrinello projector-augmented-wave (CP-PAW) code developed by Blöchl.[44] Our reaction coordinate (RC) was the C−C distance between the migrating CH_3 group and the carbonyl carbon. Figure 3 displays the free energy profile calculated according to eq 1 as a function of RC. Also shown are the calculated values (CP-PAW) for $\Delta G^{\ddagger}$, $\Delta H^{\ddagger}$, and $\Delta S^{\ddagger}$ compared to experimental results (Exp) and estimates from static ADF calculations (ADF). We note that CP-PAW and ADF afford similar $\Delta G^{\ddagger}$ values. However, the

Table 4. Computed Heat of Reaction[a] for the CO Insertion in $[M(CO)_2I_2(CH_3)L]^{n-}$

M	L[b]	ΔS(g)[c]	ΔH(g)[c]	ΔG(g)[c]	ΔH(s)[d,e]	ΔG(s)[d,f]
Ir		−0.02	8.02	8.03	7.12	7.13
	I$^-$	3.62	3.54	2.46	4.02	2.94
	CO	−7.24	−2.92	−0.76	−4.29	−2.13
	P$(OCH_3)_3$	−2.59	0.60	1.37	−4.24	−3.47
Rh		0.63	−1.69	−1.88	−2.09	−2.28
	I$^-$	2.29	−6.13	−6.81	−5.56	−6.24
		(−12.9)[g]			(−8.84)[g]	(−5.00)[g]
	CO	−7.09	−8.91	−6.80	−10.72	−8.60

[a] At 298.15 K and 1 atm. All energies are in kcal mol^{-1} and entropies in cal K^{-1} mol^{-1}. Reaction takes place from a reactant isomer (**2a**) to the most stable product isomer (**3c**). [b] Ligand in *trans* position to methyl group. [c] ΔS(g), ΔH(g), and ΔG(g) are ΔS, ΔH, and ΔG values from gas-phase calculations. [d] Solvents are chlorobenzene for iridium and iodomethane for rhodium. [e] $\Delta H(s) = \Delta H(g) + \Delta H^{el}(s)$. Here $\Delta H^{el}(s)$ is the electrostatic solvation stabilization.[41a] [f] $\Delta G(s) = \Delta H(s) - T\Delta S(g)$. [g] Experimental numbers obtained in iodomethane.[8c]

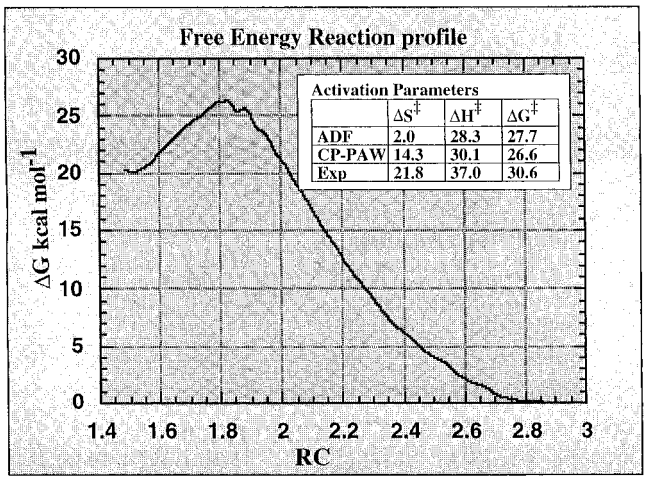

Figure 3. Free energy profile for the migratory insertion process involving $[Ir(CO)_2I_3(CH_3)]^-$ as a function of the C−C distance **b** in **TS[2-3]** (see Figure 2).

(52) Connors, K. A. *Chemical Kinetics: The Study of Reaction Rates in Solution*; VCH: New York, 1990.

(53) (a) Boudart, M.; Djega-Mariadassou, G. *Kinetics of Heterogeneous Catalytic Reactions*; Princeton University Press: Princeton, NJ, 1984. (b) Linert, W.; Kadrjawtsev, A. B. *Aust. J. Chem.* **1984**, *37*, 1139. (c) Linert, W.; Kadrjawtsev, A. B.; Schmid, R. *Aust. J. Chem.* **1983**, *36*, 1903. (d) Linert, W.; Jameson, R. F. *CSRVBR* **1989**, *18*, 477.

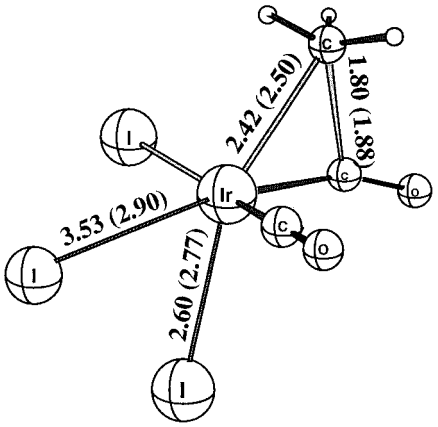

Figure 4. Optimized structures for the migratory insertion transition state **TS[2-3]** involving $[Ir(CO)_2I_3(CH_3)]^-$. Numbers in parentheses are from static ADF calculations. Numbers outside of parentheses are average values around the maximum on the free energy profile (Figure 3). All distances are in Å.

$\Delta S^{\ddagger}$ estimate from CP-PAW is now much larger and more in agreement with experiment.

The increase in $\Delta S^{\ddagger}$ for CP-PAW compared to ADF can be understood initially from Figure 4, where we have the CP-PAW and ADF transition state structures **TS[2-3]**. We note that the Ir−I bond *trans* to the emerging acyl group in the CP-PAW simulation has been elongated considerably (3.53 Å) compared to the same distance obtained from ADF calculations (2.90 Å). That the iodide ligand actually dissociates can be seen better in Figure 5, where we plot the Ir−I distances as a function of RC. We note (Figure 5A) that the Ir−I bond (**f** of Figure 5A) begins to break at the transition state (RC = 1.80) and is completely dissociated before the C−C acyl bond is finally formed (RC ≈ 1.5 Å). The Ir−I bond (Figure 5B) *trans* to the migrating methyl group undergoes large amplitude vibrations but contracts on the average by 0.2 Å after the dissociation of the bond **f** in Figure 5A. A similar contraction is observed for the third Ir−I bond, **g** of Figure 5C.

Figure 6 displays the corresponding changes in the three Ir−C bond distances. The Ir−CH_3 linkage (**a** of Figure 6A) is not completely broken after the transition state at RC = 1.6 Å. At this point the Ir−C bond of the emerging acyl ligand has been elongated by an average of 0.15 Å, as the ability of the CO group to accept electron density from the metal has been reduced. The reduction in π-acceptor ability of the CO group on the acyl ligand is compensated for by an increase in back-donation from the metal to the remaining CO ligand. As a result, the Ir−CO distance (**h** of Figure 6B) contracts by an average of 0.07 Å. The increase in back-donation is also manifested in the increase in the CO distance (**i** of Figure 7A) for the remaining CO ligand. The reduction in the formal bond order for the CO group of the emerging acyl ligand from 3 to 2 results in an even larger CO elongation, **d** of Figure 7A. We note finally the change in the Ir−C−O bond angle (**cd** of Figure 7) from 180 to 110° with an onset from before the transition state at RC = 2.0.

The dissociation of a M−I bond during the migratory insertion is unique to iridium. The corresponding rhodium system exhibits long-amplitude vibrations for all

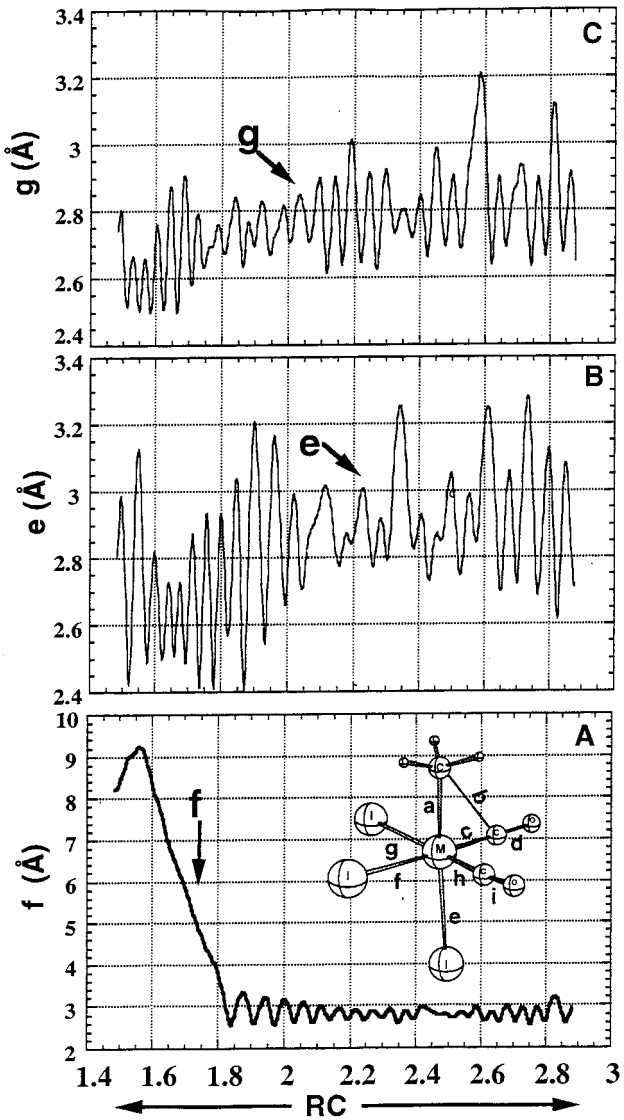

Figure 5. Changes in the Ir−I bond distances during the insertion process as a function of the reaction coordinate (RC) represented by the C−C bond distance.

three Rh−I bonds during the CP-PAW simulation of the insertion process; however, the Rh−I bonds remain intact. The dissociation of the Ir−I bond is driven entirely by entropy, which overcomes the remaining Ir−I bond strength (ΔH < 10 kcal mol^{-1}) in the transition state.

2. Migratory Insertion Involving $[M(CO)_2I_2L(CH_3)]^{n-}$ (M = Rh, Ir; *n* = 0, 1). A. Thermochemistry for the Substitution of I^- in $[M(CO)_2I_3(CH_3)]^-$ (M = Rh, Ir) *trans* to Methyl by Other Ligands L. As suggested by both Forster[12] and Maitlis et al.,[19] the oxidative addition product $[M(CO)_2(CH_3)I_3]^-$ (**2** of Scheme 1) could undergo ligand substitution prior to migratory insertion, depending on the reaction conditions. Therefore, to understand the migratory insertion as a whole, we have to include the preequilibrium substitution steps of eqs 3 and 4.

$$[M(CO)_2I_3(CH_3)]^- \rightarrow [M(CO)_2I_2(CH_3)] + I^- \quad (3)$$

$$[M(CO)_2I_2(CH_3)] + L \rightarrow [M(CO)_2I_2L(CH_3)]^{n-} \quad n = 0, 1 \quad (4)$$

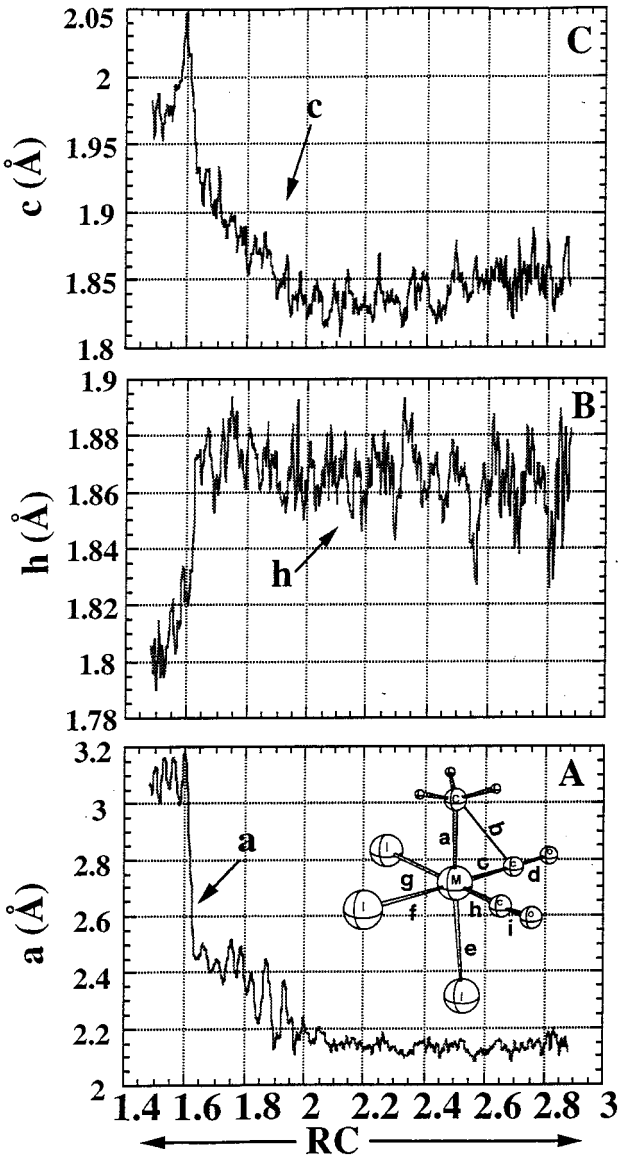

Figure 6. Changes in the Ir−C bond distances during the insertion process as a function of the reaction coordinate (RC) represented by the C−C bond distance.

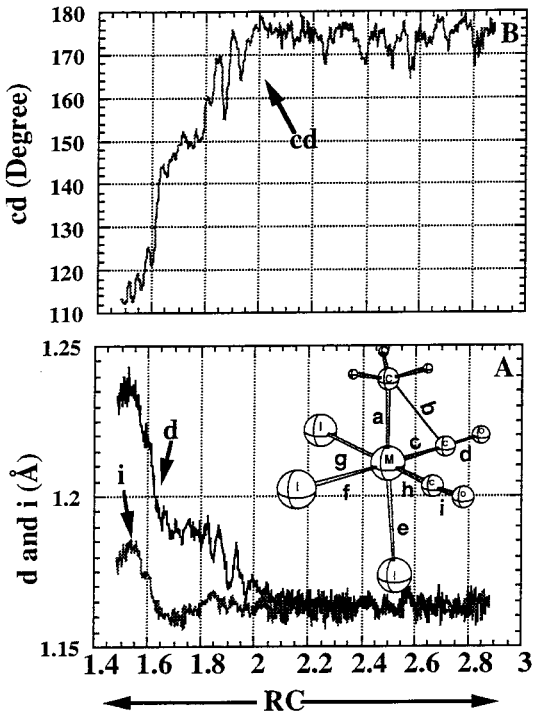

Figure 7. Changes in the CO bond distances and Ir−C−O bond angle during the insertion process as a function of the reaction coordinate (RC) represented by the C−C bond distance.

Table 5. Computed Reaction Thermodynamics[a] for the Dissociation and Substitution of I^- in $[M(CO)_2I_3(CH_3)]^-$

reacn[b]	ΔS(g)[c]	ΔH(s)[d,e]	ΔG(s)[d,f]
I → ***II*** + I^-	30.8	20.6	11.4
	30.8[g]	17.2[g]	8.0[g]
I + CH_3***O***H → ***III*** + I^-	−8.8	11.4	14.0
I + CH_3C(***O***)OH → ***IV*** + I^-	−7.6	13.1	15.4
I + ***C***O → ***V*** + I^-	−5.8	4.0	5.7
I + ***P***$(OCH_3)_3$ → ***VI*** + I^-	−25.2	−7.4	0.1
I + ***Sn***I_3^- → ***VII*** + I^-	−18.8	0.2	5.8
VIII → ***IX*** + I^-	28.5	15.4	6.9
VIII + ***C***O → ***X*** + I^-	−6.4	4.3	6.2

[a] At 298.15 K and 1 atm. All energies are in kcal mol^{-1} and entropies in cal K^{-1} mol^{-1}. [b] The Roman numbering code associated with each complex refers to the index in Table 1. [c] ΔS(g) is the ΔS value from gas-phase calculations. [d] In chlorobenzene for iridium complexes and in iodomethane for rhodium complexes. [e] ΔH(s) = ΔH(g) + ΔH^{el}(s). Here ΔH(g) is the ΔH value from gas-phase calculations and ΔH^{el}(s) is the electrostatic solvation stabilization.[41a] [f] ΔG(s) = ΔH(s) − $T\Delta S$(g). [g] In 25% CH_3OH−PhCl.

Dissociation of the iodide ligand is endothermic by 20.6 kcal mol^{-1} (Ir) and 15.4 kcal mol^{-1} (Rh) in chlorobenzene ($\epsilon_0 = 5.6$) and iodomethane ($\epsilon_0 = 7.0$), respectively, as shown in Table 5. Thus, in solvents of similar polarity, the Ir−I bond is seen to be stronger by 5.2 kcal mol^{-1}, again due to the relativistic bond stabilization. The corresponding free energies of dissociation are 11.4 kcal mol^{-1} (Ir) and 6.9 kcal mol^{-1} (Rh). This would indicate that the equilibrium is to the left in eq 3 for moderately polar solvents ($\epsilon_0 < 10$). Increasing the solvent polarity by adding 25% methanol decreases the dissociation enthalpy for iridium to 8.0 kcal mol^{-1} (Ir), whereas the same value in neat methanol is 7.4 kcal mol^{-1} (Ir). The free energy of dissociation for the process in eq 3 (ΔG_3) can be considered as an upper bound to $\Delta G^{\ddagger}$ for a dissociative substitution of the I^- ligand in $[Ir(CO)_2I_3(CH_3)]^-$ *trans* to methyl by another ligand L (eqs 3−4). Our calculated ΔG_3 values (Table 5) would indicate that such a process is kinetically feasible in more polar solvents, especially for rhodium. We note that the solvent used under industrial conditions is neat methanol ($\epsilon_0 = 32.6$).

The intermediate complex $[M(CO)_2I_2(CH_3)]$ formed in eq 3 can undergo isomerization before capture of another ligand L. As a result, eq 4 can give rise to different isomers of $[M(CO)_2(CH_3)I_2L]^{n-}$. We consider initially only the isomer where L is in a *trans* position to the methyl group. Optimized structures for $[M(CO)_2(CH_3)I_2L]^{n-}$ are given in Tables 1 and 2 whereas thermodynamic data on the complete substitution reaction (eqs 3 and 4) can be found in Table 5.

The oxygen donors CH_3OH and $CH_3C(O)OH$ are hard ligands that only form weak bonds to iridium with bond dissociation energies (ΔH_4) of 9.2 kcal mol^{-1} (CH_3OH) and 7.5 kcal mol^{-1} ($CH_3C(O)OH$). The corresponding

substitution reactions are, as a result, highly endergonic (Table 5) with calculated free energies of 14.0 kcal mol^{-1} (CH_3OH) and 15.4 kcal mol^{-1} ($CH_3C(O)OH$), respectively. Our calculations would indicate that I^- is unlikely to be displaced by CH_3OH or $CH_3C(O)OH$ to any appreciable degree, even in neat methanol under industrial conditions.

The softer ligands L = CO, $P(OCH_3)_3$, SnI_3^- form bonds with iridium comparable in strength to that of the Ir−I linkage, with dissociation energies of 16.6 kcal mol^{-1} (CO), 28.0 kcal mol^{-1} ($P(OCH_3)_3$), and 20.4 kcal mol^{-1} (SnI_3^-). The corresponding substitution reactions (in chlorobenzene) are slightly endergonic with free energies of 5.7 kcal mol^{-1} (CO), 0.1 kcal mol^{-1} ($P(OCH_3)_3$), and 5.8 kcal mol^{-1} (SnI_3^-). These numbers can be reduced further in neat methanol by 4 kcal mol^{-1}. Thus, under industrial conditions, I^- could be displaced to an appreciable degree by other soft ligands.

The variable strength of the Ir−L bonds is reflected clearly in the length of the Ir−CH_3 linkage *trans* to the ligand L, in Table 1. For the oxygen donors CH_3OH and $CH_3C(O)OH$ with weak Ir−L bonds, the Ir−CH_3 distance is relatively short (2.13 Å). On the other hand, the more strongly coordinating ligands CO, $P(OCH_3)_3$, and SnI_3^- give rise to an elongation of the Ir−CH_3 linkage with the longest distance (2.19 Å) for the ligand ($P(OCH_3)_3$) with the strongest Ir−L bond. The influence of L on the Ir−CH_3 bond will be important in the next section, when we discuss the migratory aptitude of the methyl group.

B. Influence of the Ligand L on Migratory Insertion Rate. The salient structural features of the migratory insertion process

$$\underset{\mathbf{2}}{[M(CO)_2I_2L(CH_3)]^{n-}} \rightarrow \mathbf{TS[2\text{-}3]} \rightarrow \underset{\mathbf{3}}{[M(CO)I_2L(COCH_3)]^{n-}} \qquad n = 0, 1 \quad (5)$$

with L = CH_3OH, $CH_3C(O)OH$, CO, $P(OCH_3)_3$, SnI_3^- are quite similar to those already discussed for L = I^- in the previous sections (see Tables 1 and 2 and Figure 2).

During the insertion the M−CH_3 and CH_3−CO distances vary more appreciably than any other bond length. The M−CH_3 bond lengths increase from 2.13 to 2.19 Å in **2** to 2.35−2.50 Å in **TS[2-3]** (see Tables 1 and 2 and Figure 6A), whereas the CH_3−CO distances decrease from 2.77 to 2.87 Å in **2** to 1.70−1.92 Å in **TS[2-3]**. The M−CO bond to which the methyl group is migrating does not change its length much during the reaction. This underlines that the reaction in eq 5 primarily occurs with a migration of the alkyl group toward the CO ligand rather than an insertion of CO into the Ir−CH_3 bond.

The M−L bond *trans* to the methyl group is seen to become shorter by 0.12−0.31 Å as the methyl group migrates and leave L without competition for bonding with d orbitals along the Ir−L vector. At the same time the Ir−I bond *trans* to the emerging acyl ligand is seen to increase (0.1 Å) as the *trans* effect of the $CH_3C(O)$ group manifests itself increasingly toward the transition state **TS[2-3].** We note finally that the bending of the M−C−O angle from 180° in **2** to 160−150° in **TS[2-3]** results in a loss of metal-to-CO π^* back-donation. This results in a modest elongation of the Ir−CO and C−O bonds (see Table 1 and Figures 6 and 7).

The most direct influence of the ligand L on the migratory insertion barrier is through its *trans*-directing ability to labilize the Ir−CH_3 bond in **2** and thus facilitate the breakage of this bond during the methyl migration. For the two oxygen donors L = CH_3OH, $CH_3C(O)OH$, where the *trans* influence is modest and the Ir−CH_3 bonds short (2.13 Å), we calculate high free energies of activation given by 34.8 kcal mol^{-1} (CH_3OH) and 35.6 kcal mol^{-1} ($CH_3C(O)OH$)), respectively. One might have expected a similar high value for $\Delta G^{\ddagger}$ in the case $[M(CO)_2I_2(CH_3)]$, where the position *trans* to the methyl in **2** is vacant (compound ***II***). However, the lack of initial labilization of the Ir−CH_3 bond is compensated for by the transit of an iodide ligand from the position *trans* to the emerging acyl ligand to the position *trans* to the departing methyl group. In this transit the iodide avoids the *trans* labilization of the emerging acyl while making full use of the enhanced Ir−I interaction made possible by the departing methyl. The free energy of activation for the migration in $[M(CO)_2I_2(CH_3)]$ was calculated to be 22.7 kcal mol^{-1}, much lower than for the oxygen donors L = CH_3OH, $CH_3C(O)OH$.

The free energy of activation for the migration reactions involving the three strongly *trans* labilizing ligands L = CO, $P(OCH_3)_3$, SnI_3^- were all calculated to be lower than for L = I^- with values of 18.5 kcal mol^{-1} (CO), 13.3 kcal mol^{-1} ($P(OCH_3)_3$), and 23.3 kcal mol^{-1} (SnI_3^-), respectively, as shown in Table 3. On the basis of the optimized Ir−CH_3 distances in **2** for the three ligands one might have expected $\Delta G^{\ddagger}$ for L = SnI_3^- to be on a par with $\Delta G^{\ddagger}$ for L = CO. However, CO and $P(OCH_3)_3$ are both π acceptors that can compensate for the loss of metal-to-CO π^* back-donation as the M−C−O angle bends from 180° in **2** to 160−150° in **TS[2-3].** This option is not available for L = SnI_3^-.

The free energy of activation for the methyl migration in $[M(CO)_2I_2L(CH_3)]^{n-}$ with L *trans* to methyl follows the order

$$P(OCH_3)_3 > CO > SnI_3^-, \text{none} > I^- > CH_3OH, CH_3C(O)OH$$

with respect to the ligand L. This order is to a first approximation determined by the ability of L to labilize the M−CH_3 bond *trans* to it. The order is further shaped by the ability of the π acceptors L = CO, $P(OCH_3)_3$ to stabilize the transition state and, in the case of L = none, by the relocation of an iodide ligand to the site *trans* to the migrating methyl group.

We have up to this point considered the isomer of $[M(CO)_2I_2L(CH_3)]^{n-}$, for which L is in a position *trans* to the migrating methyl group. The *trans* position allows for optimal influence on the rate of methyl migration through *trans* labilization of the Ir−CH_3 bond. We find for L = CO, $P(OCH_3)_3$ substantial reductions in $\Delta G^{\ddagger}$ compared to L = I^- of 9.2 kcal mol^{-1} (CO) and 14.4 kcal mol^{-1} ($P(OCH_3)_3$). This is qualitatively in line with the observed reductions of 6.8 kcal mol^{-1} (CO) in Table 3. Quantitatively, our results differ from experiment because $[M(CO)_2I_2L(CH_3)]^{n-}$ might also exist as isomers where L is *cis* to the migrating methyl. This point will be dealt with in the next section.

Table 6. Methyl Migration Activation Parameters[a] for the Different Isomers of $[Ir(CO)_3I_2(CH_3)]$

isomer	$\Delta S^{\ddagger}$(g)[b]	$\Delta H^{\ddagger}$(g)[b]	$\Delta G^{\ddagger}$(g)[b]	G_{rel}(g)[c]	$\Delta H^{\ddagger}$(s)[d,e]	$\Delta G^{\ddagger}$(s)[d,f]	G_{rel}(s)[c,d]	$\Delta S^{\ddagger}$(exptl)[d]	$\Delta H^{\ddagger}$(exptl)[d]	$\Delta G^{\ddagger}$(exptl)[d]
fac,cis	−3.90	18.7	19.8	0	17.3	18.5	0	−8.6 ± 1.9[g]	21.3 ± 0.7[g]	23.8 ± 0.7[g]
mer,cis	−1.19	30.2	30.5	−0.95	28.8	29.2	−1.77			
	−4.34[h]	25.2[h]	26.5[h]		24.1[h]	25.4[h]				
mer,trans	−0.46	18.4	18.5	−0.72	16.8	16.9	+0.35			

[a] At 298.15 K and 1 atm. All energies are in kcal mol^{-1} and entropies in cal K^{-1} mol^{-1}. [b] $\Delta S^{\ddagger}$(g), $\Delta H^{\ddagger}$(g), and $\Delta G^{\ddagger}$(g) are $\Delta S^{\ddagger}$, $\Delta H^{\ddagger}$, and $\Delta G^{\ddagger}$ values from gas-phase calculations. [c] Calculated thermodynamic free energies relative to the *fac,cis* isomer. [d] Experimental numbers are obtained in chlorobenzene. The same solvent is used in theoretical calculations. [e] $\Delta H^{\ddagger}(s) = \Delta H^{\ddagger}(g) + \Delta H^{el}(s)$. Here $\Delta H^{el}(s)$ is the electrostatic solvation stabilization.[41a] [f] $\Delta G^{\ddagger}(s) = \Delta H^{\ddagger}(s) - T\Delta S^{\ddagger}(g)$. [g] Reference 8a. [h] Methyl group is migrating to the CO group which is in a *trans* position to another CO group.

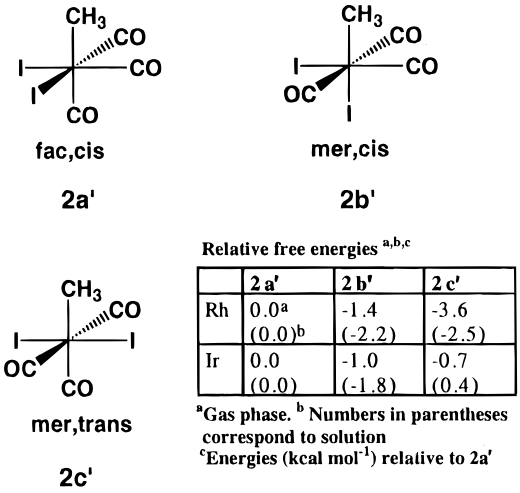

Figure 8. Isomers of $[M(CO)_3I_2(CH_3)]$ (M = Rh, Ir) and their relative energies.

We close the discussion here by observing that our calculations point to substantial rate enhancements in methyl migration for catalysts in which strongly labilizing ligands by design are positioned *trans* to the $M-CH_3$ bond. Finally, the rate enhancement obtained for $L = SnI_3^-$ might explain the use of SnI_2 as promoters in methanol carbonylation if we assume that SnI_2 inserts into the Ir−I bond *trans* to the methyl group.

C. Rate of Methyl Migration for Different Isomers of $[Ir(CO)_2I_2L(CH_3)]$ for L = CO. We shall finally discuss how the rate of methyl migration is influenced by placing L at different positions relative to the methyl group. The discussion will be based on $[Ir(CO)_2I_2L(CH_3)]^{n-}$ with L = CO, for which we have the three possible isomers **2a′** (*fac,cis*), **2b′** (*mer,cis*), and **2c′** (*mer,trans*), as shown in Figure 8. It follows from our calculations that the isomer **2b′** with iodide *trans* to the methyl group is more stable by 2 kcal mol^{-1} than the two isomers **2a′** and **2c′** with CO in the *trans* positions, as shown in Table 6.

Migration in the more stable **2b′** isomer with iodide *trans* has two possible pathways that both, as expected, have higher $\Delta G^{\ddagger}$ values than migration in the two isomers **2a′** and **2c′** with CO *trans* to methyl. However, methyl migration to a CO* with another CO_t ligand *trans* is favored (25.5 kcal mol^{-1}) over migration to a CO* with an iodide ligand *trans* (29.2 kcal mol^{-1}), as shown in Table 6. In the former case CO_t can more directly make up for the loss of metal-to-CO* backdonation as the M−C−O* angle decreases, since the two CO ligands are interacting with the same d_π orbital. For the less stable isomers **2a′** and **2c′** with CO and methyl *trans* we find, as expected, lower barriers. Here too migration to CO* with a CO *trans* is more favorable, 16.9 kcal mol^{-1} (**2c′**), than migration to CO* with iodide *trans*, 18.5 kcal mol^{-1} (**2a′**), as shown in Table 6. Given the preference for isomer **2b′**, it seems reasonable to compare the lower $\Delta G^{\ddagger}$ value of 25.4 kcal mol^{-1} to the experimental estimate of 23.8 kcal mol^{-1} in Table 6. However, the experimental value might also reflect a Boltzmann-weighted average of $\Delta G^{\ddagger}$ values for the migration from several of the isomers. The important observation is that the $-T\Delta S^{\ddagger}$ term is more positive in experimental value than its calculated result for **2a′**. In the case of $[Ir(CO)_2I_3Me]^-$, the experimental result gives a more negative $-T\Delta S^{\ddagger}$ term than the ADF result, because elongation of the metal−iodide bond *trans* to the emerging acyl group progressed substantially in the transition state. However, in the case of **2b′**, which is the major component under experimental conditions, there is no iodide ligand which can be *trans* to the emerging acyl group when more favorable methyl migration to CO* with another CO_t ligand *trans* occurs. This will give a more positive $-T\Delta S^{\ddagger}$ term, as observed.

We have not analyzed the relative stabilities of the six possible isomers of $[Ir(CO)_2(P(OCH_3)_3)I_2(CH_3)]$. However, we expect the experimental $\Delta G^{\ddagger}$ values to reflect migrations from several isomers with a predominance from isomers where iodide is *trans* to the methyl group. Finally, for $[Rh(CO)_3I_2(CH_3)]$ we find **2c′** with CO *trans* to methyl to be comparable in energy to **2b′** with iodide *trans* in solution, as shown in Figure 8. Thus, in this case the $\Delta G^{\ddagger}$ value of migration should be considerably lower for $[Rh(CO)_3I_2(CH_3)]$ compared to $[Rh(CO)_2I_3(CH_3)]^-$.

Concluding Remarks

We have carried out a detailed study on the migratory insertion reaction process $[M(CO)_2I_3(CH_3)]^- \rightarrow [M(CO)I_3(COCH_3)]^-$ (M = Rh, Ir). The study was based on static and dynamic DFT calculations.

The calculated free energies of activation ($\Delta G^{\ddagger}$) are 27.7 kcal mol^{-1} (Ir) and 17.2 kcal mol^{-1} (Rh), in good agreement with the experimental estimates at 30.6 ± 1.0 kcal mol^{-1} (Ir) and 19.3 ± 0.5 kcal mol^{-1} (Rh), respectively. The higher barrier for M = Ir is attributed to a relativistic stabilization of the $Ir-CH_3$ bond. It is indicated that enthalpic and entropic contributions to $\Delta G^{\ddagger}$ can vary considerably depending on reaction conditions without changing $\Delta G^{\ddagger}$ considerably. Especially, simulations based on ab initio molecular dynamics (AIMD) underlined that the reaction system might prefer to trade entropy for enthalpy in polar solutions by dissociating an I^- ligand for M = Ir.

A systematic study was also carried out on the general methyl migration reaction $[Ir(CO)_2I_2L(CH_3)]^{n-} \rightarrow [Ir(CO)I_2L(COCH_3)]^{n-}$ ($n = 0, 1$), in which an iodide ligand *trans*

to methyl is replaced by another ligand L (where L = CH_3OH, $CH_3C(O)OH$, CO, $P(OCH_3)_3$, SnI_3^-) or an empty coordination site. The free energies of activation for the methyl migration in $[Ir(CO)_2I_2L(CH_3)]^{n-}$ with L *trans* to methyl follow the order $P(OCH_3)_3 > CO > SnI_3^-$, none $> I^- > CH_3OH$, $CH_3C(O)OH$, with respect to the ligand L. This order is to a first approximation determined by the ability of L to labilize the $M-CH_3$ bond *trans* to it. The order is further shaped by the ability of the π acceptors L = CO, $P(OCH_3)_3$ to stabilize the transition state and, in the case of L = none, by the relocation of an iodide ligand to the site *trans* to the migrating methyl group. It is finally discussed how placing L *cis* to the migrating CH_3 group might influence the migratory aptitude of methyl.

Acknowledgment. M.C. is pleased to acknowledge financial support by Kyung Hee University for a sabbatical leave at the University of Calgary. This work has been supported by the National Science and Engineering Research Council of Canada (NSERC).

Supporting Information Available: Listings giving optimized geometries of the crucial structures reported (Cartesian coordinates, in Å). This material is available free of charge via the Internet at http://pubs.acs.org.

OM9910221